

RX J2130.6+4710 – an eclipsing white dwarf–M-dwarf binary star. ^{*}

P. F. L. Maxted^{1,2}, T. R. Marsh^{3,2}, L. Morales-Rueda^{4,2}, M. A. Barstow⁵
P. D. Dobbie⁵, M. R., Schreiber⁶, V. S. Dhillon⁷ and C. S. Brinkworth²

¹*School of Chemistry & Physics, Keele University, Staffordshire, ST5 5BG, UK.*

²*University of Southampton, Department of Physics & Astronomy, Highfield, Southampton, S017 1BJ, UK.*

³*Department of Physics, University of Warwick, Coventry, CV4 7AL, UK.*

⁴*Department of Astrophysics, Faculty of Science, University of Nijmegen, P.O. Box 9010, 6500 GL Nijmegen, The Netherlands.*

⁵*Department of Physics & Astronomy, University of Leicester, University Road, Leicester LE1 7RH, UK.*

⁶*Université Louis Pasteur, Observatoire de Strasbourg, 11 rue de l'Université, 67000 Strasbourg, France*

⁷*Department of Physics and Astronomy, University of Sheffield, Sheffield, S3 7RH*

Accepted — Received —

ABSTRACT

We report the detection of eclipses in the close white-dwarf–M-dwarf binary star RX J2130.6+4710. We present lightcurves in the B, V and I bands and fast photometry obtained with the three channel CCD photometer Ultracam of the eclipse in the u' , g' and r' bands. The depth of the eclipse varies from 3.0 magnitudes in the u' band to less than 0.1 magnitudes in the I band. The times of mid-eclipse are given by the ephemeris $\text{BJD}(\text{Mid-eclipse}) = 2\,452\,785.681876(2) + 0.521\,035\,625(3)E$, where figures in parentheses denote uncertainties in the final digit. We present medium resolution spectroscopy from which we have measured the spectroscopic orbits of the M-dwarf and white dwarf. We estimate that the spectral type of the M-dwarf is M3.5Ve or M4Ve, although the data on which this is based is not ideal for spectral classification. We have compared the spectra of the white dwarf to synthetic spectra from pure hydrogen model atmospheres to estimate that the effective temperature of the white dwarf is $T_{\text{eff}} = 18\,000 \pm 1000$ K. We have used the width of the primary eclipse and duration of totality measured precisely from the Ultracam u' data combined with the amplitude of the ellipsoidal effect in the I band and the semi-amplitudes of the spectroscopic orbits to derive masses and radii for the M-dwarf and white dwarf. The M-dwarf has a mass of $0.555 \pm 0.023 M_{\odot}$ and a radius of $0.534 \pm 0.053 R_{\odot}$, which is a typical radius for stars of this mass. The mass of the white dwarf is $0.554 \pm 0.017 M_{\odot}$ and its radius is $0.0137 \pm 0.0014 R_{\odot}$, which is the radius expected for a carbon-oxygen white dwarf of this mass and effective temperature. The lightcurves are affected by frequent flares from the M-dwarf and the associated dark spots on its surface can be detected from the distortions to the lightcurves and radial velocities. RX J2130.6+4710 is a rare example of a pre-cataclysmic variable star which will start mass transfer at a period above the period gap for cataclysmic variables.

Key words: stars: binaries: close – stars: white dwarfs – stars: fundamental parameters – stars: binaries: eclipsing – stars: individual: RX J2130.6+4710

1 INTRODUCTION

RX J2130.6+4710 is a soft X-ray source which was detected in a survey of the galactic plane by the ROSAT satellite (Trümper 1983, Motch et al. 1991). Motch et al. (1997) used optical spectroscopy of stars near the position of these X-ray sources to identify and classify optical counterparts in the region of the Cygnus constellation.

^{*} Based on observations made with William Herschel, Isaac Newton and Jacobus Kapteyn telescopes operated on the island of La Palma by the Royal Greenwich Observatory in the Spanish Observatorio del Roque de los Muchachos of the Instituto de Astrofísica de Canarias.

RX J2130.6+4710 was identified with a faint star which they labelled RX J2130.3+4709 about 12 arcsec SSE of the bright G0 star HD 204906 (=SAO 50947, $V=8.45$). The spectrum of RX J2130.6+4710 shows the broad Balmer lines of a typical DA white dwarf together with narrow emission lines in the cores in the Balmer lines and the Ca II H&K lines. Also visible are molecular bands of TiO from the Me-type companion star which is also the source of the narrow emission lines. They classified RX J2130.6+4710 as a WD+Me close binary star. Motch et al. report that the radial velocities of broad Balmer lines and emission lines move in opposite directions with an orbital period of approximately 12 hours. The white dwarf is too cool to contribute to the X-ray flux (1.6×10^{-2} ctss $^{-1}$) which probably arises from the Me star companion. The distance from the optical counterpart to catalogued position of the X-ray source is almost exactly the same as the 90% confidence radius of 26.1 arcsec in the position of the X-ray source.

It is likely that RX J2130.6+4710 is the same source as the 2E 2128.4+4657, a soft X-ray source detected by the Einstein satellite which was identified with HD 204906 by Thompson, Shelton & Arning (1998). The position of 2E 2128.4+4657 given in the Einstein Observatory catalog (Harris et al. 1994) differs by 23 arcsec from the position for the optical counterpart of RX J2130.6+4710 given by Motch et al., which is comfortably within the positional uncertainty of 42 arcsec for the X-ray source. We note that RX J2130.6+4710 appears in the ‘‘Catalogue of cataclysmic binaries, low-mass X-ray binaries and related objects’’ (Ritter & Kolb 1998) as ‘‘J2130+4710’’. The corresponding name in the SIMBAD database (Wenger et al. 2000) is RX J2130.6+4710, which is a more accurate reflection of the position of the optical counterpart ($\alpha = 21^{\text{h}}30^{\text{m}}18.6^{\text{s}}$, $\delta = +47^{\circ}10'08''$, J2000.0) and is the name we use throughout this paper.

White dwarf stars are the remnants of stars less massive than about $5-8M_{\odot}$ which have been through the red giant phase of their evolution. The separation of a WD+Me binary with a period of 12 hours is $2-3R_{\odot}$, which is much smaller than the typical size of a red giant ($\sim 100-1000R_{\odot}$). This suggests that RX J2130.6+4710 is a post-common envelope binary (PCEB). In this scenario, the expanding red giant star comes into contact with its Roche lobe and begins to transfer mass to its companion star. This mass transfer is highly unstable, so a common envelope forms around the companion and the core of the red giant. The drag on the companion orbiting inside the common envelope leads to extensive mass loss and dramatic shrinkage of the orbit (Iben & Livio 1993). Common-envelope (CE) evolution affects the evolution of many binary stars and can produce some of the most dramatic objects known, including low-mass and high-mass X-ray binaries, novae, supernovae and AM CVn binaries. However, it is a poorly understood process, so it is useful to study relatively simple PCEBs like RX J2130.6+4710 to see what they can tell us about this phenomenon.

RX J2130.6+4710 is one of a very small sample of eclipsing white dwarfs with companions that can be directly detected in the optical spectrum. These binaries offer a rare opportunity to accurately measure the properties of low mass stars and white dwarfs. In this paper we report photometric and spectroscopic observations of RX J2130.6+4710. We

Table 1. Exposure times, T_{exp} , for observations of RX J2130.6+4710 obtained with the JKT. N is the number of useful images obtained.

| Filter | N | T_{exp} (s) |
|--------|------|----------------------|
| U | 6 | 120 |
| B | 1002 | 6.5–60 |
| V | 536 | 30 |
| R | 6 | 20 |
| I | 581 | 30 |

have used these to measure the masses and radii of the white dwarf and the M-dwarf to an accuracy of about 5 per cent. We find that the white dwarf in RX J2130.6+4710 is a typical carbon-oxygen white dwarf and that the M-dwarf has a normal radius for its mass.

2 OBSERVATIONS & REDUCTIONS

2.1 Photometry

We first observed RX J2130.6+4710 using the 1m Jacobus Kapteyn telescope (JKT) on the Island of La Palma. We obtained 478 images with an I band filter and 520 images with a V-band filter using a TEK charge coupled device (CCD) during the interval 1998 Aug 5–9. The exposure times were 1.5–3 s for the I band images and 1.5–5 s for the V-band images. The image scale on the CCD was 0.33 arcsec per pixel. Our intention was to confirm the orbital period of the binary from the sinusoidal reflection effect due to the irradiation of one side of the M-dwarf by the white dwarf. We were delighted to find that the V-band images show an eclipse 0.6 magnitudes deep lasting about 30 minutes occurring at about 0030UT 1998 Aug 10. The I band images show an eclipse about 0.1 magnitudes deep at the same time. This is exactly what would be expected for the eclipse of a white dwarf by an M-dwarf with a similar luminosity in the V-band.

We obtained further photometry of RX J2130.6+4710 with the JKT during the interval 2000 August 16–22 using a SITE CCD, which gives the same image scale as the TEK CCD. Images were obtained using Harris UBVR filters. The number of images secured with each filter and exposure times are given in Table 1. The shorter exposures with the B filter were used for observations during eclipses of RX J2130.6+4710.

Primary eclipses of RX J2130.6+4710 were observed with ULTRACAM and the WHT on the nights of 17 May 2002, 24 May 2003 and 25 May 2003. Attempts to observe the secondary eclipse on 19 May 2002 and 13 November 2003 were compromised by poor seeing and flaring of the M-dwarf. We have subsequently discovered that the secondary eclipse is likely to be extremely shallow (see later) so we do not discuss these observations further in this paper.

ULTRACAM is an ultrafast, triple-beam CCD camera. The light is split into three wavelength colours (u' , g' and r' or i') by two dichroic beam-splitters and then passes through a filter. The detectors are three back-illuminated, thinned, Marconi frame-transfer 1024×1024 active area CCD chips with a pixel scale of 0.3 arcsec pixel $^{-1}$. ULTRACAM em-

Table 2. Apparent magnitudes of RX J2130.6+4710.

| U | B | V | R | I | J | H | K _s |
|------|------|------|-------|------|-------|-------|----------------|
| 14.8 | 14.9 | 14.3 | 13.70 | 12.2 | 11.21 | 10.58 | 10.36 |

plugs frame transfer CCDs so that the dead time between exposures is negligible (24 milliseconds). Signals from Global Position System (GPS) satellites were used to ensure that the time-stamp for each image is accurate to 1 millisecond. (for further details, see Dhillon & Marsh 2001).

We reduced the data using normal extraction from fixed apertures and also Naylor’s (1998) optimal extraction from apertures varied in step with the seeing. In the latter case we used aperture radii 1.5 times the full-width at half maximum of the image of RX J2130.6+4710. RX J2130.6+4710 is located only 12 arcsec away from a much brighter G0 star so the photometry can be badly affected in poor seeing. To estimate and correct for the extent of this we placed an aperture on the sky at the same distance from the bright star as RX J2130.6+4710 and symmetrically located with respect to the diffraction spikes from this star.

The bias level in the JKT images was determined from the overscan regions and was subtracted from the image before further processing. Images of the twilight sky devoid of any bright stars were used to determine flat-field corrections by forming the median image of 3–5 twilight sky images in each filter, one for each night’s data. We used optimal photometry (Naylor 1998) to determine instrumental magnitudes of the stars in each frame. We checked for variability in the stars other than the target star in each frame before calculating differential magnitudes between RX J2130.6+4710 and a comparison star located at $\alpha = 21^h 30^m 19.7^s$, $\delta = +47^\circ 10' 26''$ (J2000.0). The mean differential magnitudes in the sense (RX J2130.6+4710 – comparison) in the B, V and I bands when RX J2130.6+4710 is not in eclipse are -0.74 , 0.29 and 0.21 , respectively.

We used an aperture with a radius of 5 pixels to measure the instrumental magnitude of RX J2130.6+4710 and the 5 standard stars in the field of PG 1633+099 with UBVR magnitudes given by Landolt (1992). We used these to calculate the apparent magnitudes for RX J2130.6+4710 given in Table 2. The calibration of our photometry is approximate because the proximity of HD 204906 to RX J2130.6+4710 makes it difficult to measure reliable fluxes. For this reason we only quote one decimal place for our apparent magnitude values. Also given in Table 2 are the infrared apparent magnitudes for RX J2130.6+4710 taken from Hoard et al. (2002).

2.2 Spectroscopy

We observed RX J2130.6+4710 with the 2.5m Isaac Newton Telescope (INT), also on the island of La Palma, using the IDS spectrograph simultaneously with our JKT observations in 2000 August. Most of our observations were obtained using a narrow slit (0.9–1 arcsec) and a 1200 line mm^{-1} grating on the 235mm camera with an EEV CCD. The spectra cover the wavelength region 3850–5500Å at a resolution of about 1.2Å and the dispersion is about 0.48Å per pixel. A typical spectrum is shown in Fig. 2. The exposure times

were 1200s and we obtained arc lamp spectra approximately once per hour to establish the wavelength scale and monitor the spectrograph drift. We also observed one eclipse of RX J2130.6+4710 with the same instrument but with a 300 line mm^{-1} grating and a 4 arcsec wide slit orientated to include the same comparison star used for the JKT photometry. The exposure times were 10 seconds and there was a 4 second delay between exposures to read out the CCD. The spectra cover the wavelength range 4215–6795 Å at a dispersion of 3.7Å per pixel.

Extraction of the narrow-slit spectra from the images was performed automatically using optimal extraction to maximize the signal-to-noise of the resulting spectra (Marsh 1989). The arcs associated with each stellar spectrum were extracted using the same weighting determined for the stellar image to avoid possible systematic errors due to the tilt of the spectra on the detector. The wavelength scale was determined from a fourth-order polynomial fit to measured arc line positions. The standard deviation of the fit to the 18 arc lines was typically 1/20 of a pixel. The wavelength scale for an individual spectrum was determined by interpolation to the time of mid-exposure from the fits to arcs taken before and after the spectrum to account for the small amount of drift in the wavelength scale ($< 0.1\text{Å}$) due to flexure of the instrument between arc spectra. We used a spectrum of BD+33 2642 obtained during the same observing run and the tabulated fluxes of Oke (1990) to determine the calibration of counts-to-flux as a function of wavelength in our spectra. No correction for slit losses was attempted but we did correct the spectra for atmospheric extinction. Statistical errors on every data point calculated from photon statistics are rigorously propagated through every stage of the data reduction.

To extract the spectrophotometry taken with a wide slit we summed the measured counts over 6 spatial pixels centered on the spectrum at every wavelength step for both RX J2130.6+4710 and the comparison star after subtracting the sky contribution estimated from a linear fit to the regions either side of the spectra. The wavelength calibration was determined from a single arc spectrum taken at the start of the night and is accurate to about 1Å.

2.3 Timing of INT and JKT data

We warn the reader here that we have not been able to establish whether the time-stamps for the data obtained with the INT and JKT are reliable. It is probable that the time-stamps for these data have an accuracy of better than 1 second. However, the observatory staff have noted that time-stamps on data such as these can be in error by a few seconds.

3 ANALYSIS

3.1 The ephemeris

We measured the time of mid-eclipse from our photometry using a least-squares fit of a very simple lightcurve model. The model is based on the eclipse of one circular disc with uniform surface brightness by another similar disc. The parameters of the model are the radii of the discs relative to

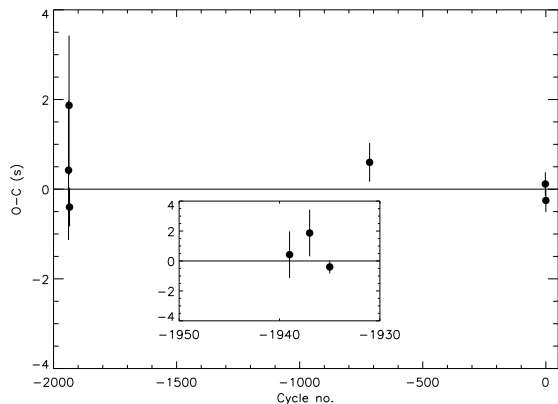


Figure 1. Residuals from a linear ephemeris for our measured times of mid-eclipse.

their maximum separation, r_1 and r_2 ; the inclination of the orbit, i ; the orbital period P and time of primary eclipse T_0 ; the luminosity ratio, l_λ ; the observed intensity outside of eclipse, I_0 and the mass ratio q . We also include a parameter to allow for a linear variation of the observed intensity with time. As we were only interested in the time of mid-eclipse, we fixed the parameters $q = 1$, $i = 90^\circ$, $P = 0.52104$ d and found the optimum values of the other parameters using the Levenberg-Marquardt method (Press et al. 1992). We fitted data covering each eclipse we had observed separately. The quality of the fits judged by-eye and from the value of χ^2 was very good (Fig. 7). The results are shown in Table 3. Corrections from UTC to Barycentric Julian date (BJD) were calculated using routines from SLALIB version 2.4-5 (Wallace 2000). The times of mid-eclipse labelled “JKT” are from B-band photometry taken with the JKT with uncertainties derived from the covariance matrix of the least-squares fit. The lightcurve for the time of mid-eclipse labelled “INT” was produced by summing the total counts over the wavelength 4215–6796Å in our low resolution spectra of RX J2130.6+4710 and the comparison then taking the ratio of these time-series. The uncertainty was also taken from the covariance matrix of the least-squares fit. The times of minimum labelled “Ultracam” are the weighted averages of the values derived by fitting the u' , g' and i' lightcurves observed with Ultracam. There is an obvious flare during the eclipse observed on 2002 May 17 so we have excluded data in the range JD= 2452412.632 to 2452412.635 from the least-square fit. The uncertainties for these values are taken from the standard deviation of the three measurements. The measurements from the three lightcurves are consistent to the individual uncertainties taken from the covariance matrix of the least-squares fit. We re-iterate our warning here that timing of the data taken with the INT and JKT presented here may be in error by a few seconds, so *these data should not be used to study the long-term period changes*.

A least-squares fit to these data gives the following linear ephemeris:

$$\begin{aligned} \text{BJD}(\text{Mid} - \text{eclipse}) &= (2452785.681876 \pm 0.000002) \\ &+ (0.521035625 \pm 0.00000003)E. \end{aligned}$$

All phases quoted in this paper have been calculated with this ephemeris.

Table 3. Times of mid-eclipse for RX J2130.6+4710.

| BJD(mid-eclipse) | Cycle | Source |
|-------------------------------|-------|------------------|
| $2451775.393803 \pm 0.000018$ | −1939 | JKT ^a |
| $2451776.435891 \pm 0.000018$ | −1937 | JKT ^a |
| $2451777.477936 \pm 0.000005$ | −1935 | INT ^a |
| $2452412.620375 \pm 0.000005$ | −716 | Ultracam |
| $2452784.639806 \pm 0.000003$ | −2 | Ultracam |
| $2452785.681873 \pm 0.000003$ | 0 | Ultracam |

^aThese data are not suitable for long-term period studies.

3.2 Spectral Type of the M-dwarf

One of our blue narrow-slit spectra was taken during a total eclipse of RX J2130.6+4710 so it only contains light from the M-dwarf. This spectrum is compared to spectra of K- and M-dwarfs taken with the same instrument and setup in Figure 2. Also shown in Figure 2 is the average of our wide-slit spectra taken during eclipse compared to spectra of M-dwarfs observed with the same instrument and setup. Spectral types for the M-dwarfs were taken from Reid, Hawley & Gizis (1995) or Hawley, Gizis & Reed (1996). We estimate that the spectral type of the M-dwarf in RX J2130.6+4710 is M3.5 or M4, based principally on the strength of the TiO bands at 5448Å, 5847Å and 6158Å and the CaOH band at 5500–60Å (Jaschek & Jaschek 1987). The spectra we have used for classification do not cover the TiO bands further to the red which are more commonly used for spectral classification and we have used only a few stars which are not standards for the comparison so the uncertainty in the classification is likely to be at least one sub-type.

3.3 Spectroscopic orbit of the M-dwarf

We used cross-correlation to measure the radial velocity of the M-dwarf from the INT spectra taken in August 2000. We first removed the contribution of the broad wings of the H β and H γ lines from the white dwarf by using two Gaussian profiles to model each line. The sum of these broad Gaussian profiles and a low order polynomial was fit to each spectrum by least squares and then subtracted from the spectrum prior to performing the cross-correlation.

We used spectra of four different M-dwarfs taken with the same instrumental setup as templates for the cross-correlation after normalization using a low-order polynomial fit by least-squares. The spectra were re-binned onto a uniform wavelength grid of 1835 pixels of 32km s^{−1} each centered on 4600Å. The cross-correlation function was calculated excluding 10Å around the two Balmer lines, which are affected by the emission lines from the cool star and the core of the spectral lines from the white dwarf. The radial velocity and its uncertainty were measured from the cross-correlation function using the method of Schneider & Young (1980) which, briefly, determines the centroid of the CCF weighted in this case by a Gaussian function with a full-width at half-maximum (FWHM) of 200km s^{−1}.

We used a least-squares fit to the measured radial velocities, V_r , of the function $V_r = \gamma_M + K_M \sin(2\pi[T - T_0]/P)$ to measure the semi-amplitude of the spectroscopic orbit for the M-star, K_M . The values of T_0 and the orbital period, P , were fixed using the ephemeris described in section 3.1.

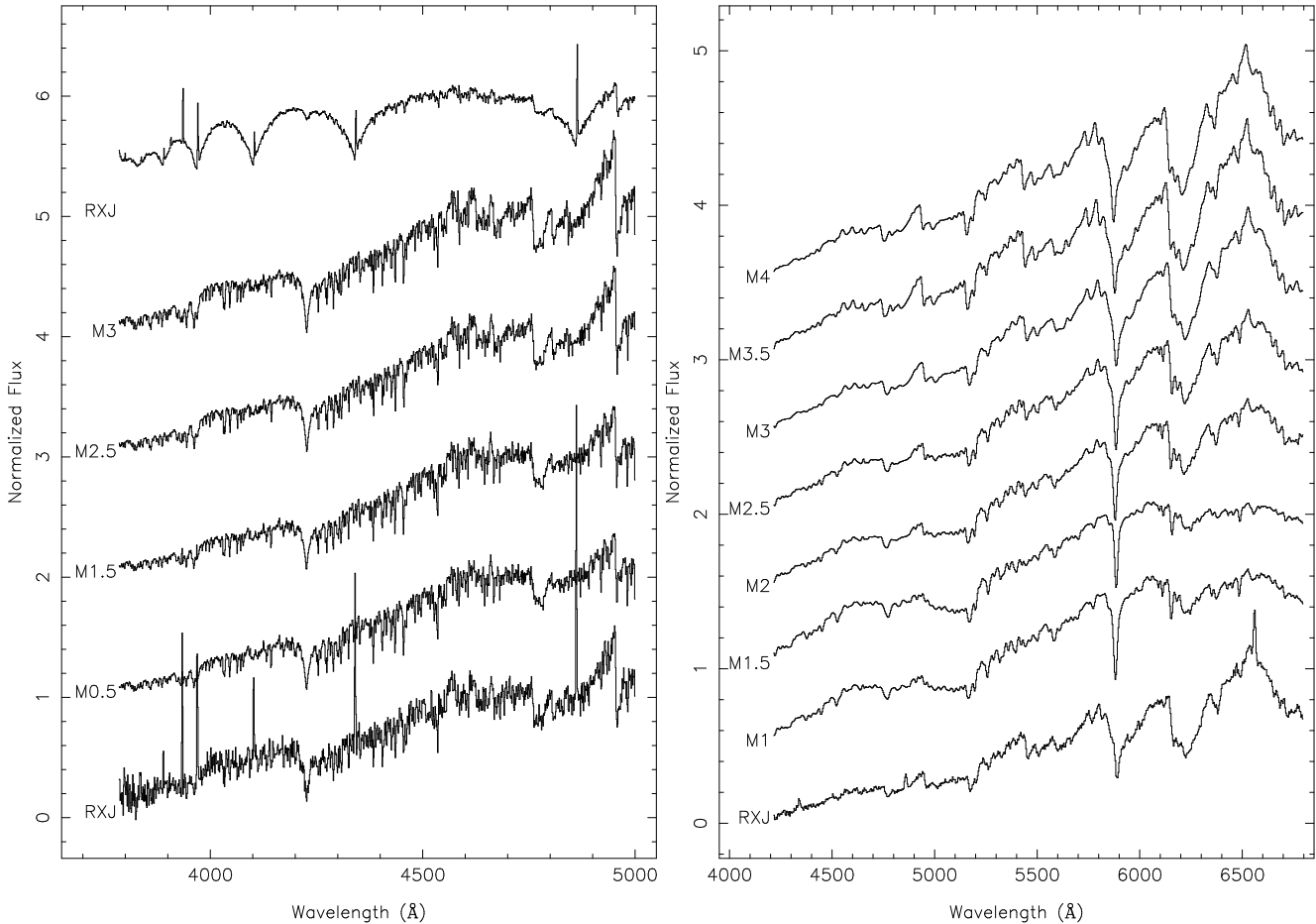


Figure 2. **Left panel** From bottom-to-top: spectrum of RX J2130.6+4710 taken at mid-eclipse, LFT 1580 (M0.5), LFT 1751 (M1.5), LFT 1466 (M2.5), LFT 93 (M3), mean of 4 spectra of RX J2130.6+4710 taken near phase 0.75. The spectra have been normalized at 5100Å and offset by 1 for clarity. **Right panel** From bottom-to-top: mean spectrum of RX J2130.6+4710 taken at mid-eclipse, LFT 1278 (M1), LFT 1436 (M1.5), LFT 1580 (M2), LFT 1751 (M2.5), LFT 1466 (M3), LFT 98 (M3.5), LFT 1431 (M4).

Table 4. Results of least-squares fits of a sine wave plus a distortion to the measured radial velocities of the M-dwarf in RX J2130.6+4710.

| Template (Sp. type) | V_{temp} (km s^{-1}) | γ_{M} (km s^{-1}) | K_{M} (km s^{-1}) | A (km s^{-1}) | ϕ_0 | ρ | σ_{sys} (km s^{-1}) | σ (km s^{-1}) |
|------------------------|---|---|--|-------------------------------|--------------------|--------------------|---|------------------------------------|
| LFT 1580 (M0.5) | -17.161 | 15.6 ± 0.7 | 135.7 ± 0.7 | 2.9 ± 0.8 | 0.18 ± 0.04 | 0.42 ± 0.07 | 3.4 | 4.5 |
| LFT 1751 (M1.5) | -27.317 | 15.5 ± 0.7 | 136.4 ± 0.7 | 2.9 ± 0.9 | 0.20 ± 0.03 | 0.40 ± 0.06 | 3.8 | 4.7 |
| LFT 1466 (M2.5) | 35.880 | 16.1 ± 0.7 | 136.7 ± 0.7 | 2.8 ± 0.9 | 0.23 ± 0.04 | 0.37 ± 0.07 | 3.9 | 4.8 |
| LFT 93 (M3) | 1.500 | 13.9 ± 0.7 | 136.7 ± 0.7 | 2.8 ± 0.9 | 0.21 ± 0.04 | 0.38 ± 0.06 | 4.0 | 4.8 |

From inspection of the residuals from these fits it was clear that there was some distortion to the radial velocities with an amplitude of a few km s^{-1} . The residuals tended to be positive over the phases $[T - T_0]/P = 0.2 - 0.4$ and negative over the phases $0.4 - 0.6$. We suspect that this distortion is due to a dark spot on the M-dwarf. We do not believe this distortion is a direct consequence of the irradiation of the M-dwarf by the white dwarf because such a distortion would be symmetrical around phase 0.5. To model this distortion we

add the term $A \sin([\phi - \phi_0]/\rho)$ to data in the phase range $\phi_0 < \phi < \phi_0 + \rho$, where $\phi = 2\pi[T - T_0]/P$. There may be a similar distortion near phase 0.9, but the data near this phase range is rather sparse so we have decided not to use a more complicated function to fit these data. The physical origin of this distortion is a dark spot crossing the observer's meridian on the visible disc of the M-dwarf at phase ϕ_{mid} . The velocity of the spot will vary as $\sin(\phi - \phi_{\text{mid}})$ and, since the inclination of the system is approximately 90°

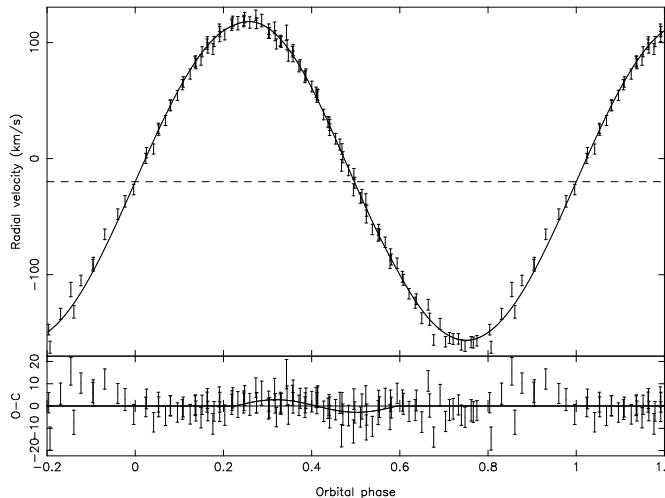


Figure 3. Radial velocities for the M-star in RXJ 2130.3+4709 measured by cross-correlation using the spectrum of LFT 1536. The upper panel shows the least-squares fit to the velocities described in the text (sine wave + distortion). The lower panel shows the residuals from the sine wave fit and the function fit by least-squares which is used to model the distortion.

its visibility will vary approximately as $\cos(\phi - \phi_{\text{mid}})$. The combination of these effects yields a distortion of the form $\sin(\phi - \phi_{\text{mid}}) \cos(\phi - \phi_{\text{mid}}) = \sin[2(\phi - \phi_{\text{mid}})]$. The effect of limb darkening will be to reduce the timescale of the variation whereas the finite size of the spot tends to increase the timescale of the distortion, so that the velocity distortion is approximately $B \sin[(\phi - \phi_{\text{mid}})/\rho]$ with $\rho \approx 0.5$. Note that $\phi_{\text{mid}} = \phi_0 + \rho/2$ so $A = -B$.

The value of χ^2 for these least-squares fits was still rather large. We therefore added an “external error”, σ_{sys} , in quadrature to the standard errors of the radial velocity measurements to account for additional sources of uncertainty. These might be instrumental, e.g., motion of the star in the slit, or intrinsic to the M-dwarf, e.g., weak emission lines, or spectral features associated with chromospheric activity such as flares or dark spots in the photosphere. The value of σ_{sys} was chosen to obtain a reduced χ^2 value of 1.

The results of the least-squares fit of the sine wave + distortion are given in Table 4. Results are given for each of the templates used for cross-correlation as listed in column 1. The value of γ_{M} has been corrected for the measured radial velocity of the template, V_{emp} , taken from Nidever et al. (2002). The spectral type of the template taken from Reid, Hawley & Gizis (1995) or Hawley, Gizis & Reed (1996) is also given. The standard deviation of the residuals, σ is given in the final column. An example of the measured radial velocities and the function fit by least-squares is shown in Fig. 3.

We adopt the weighted mean values from Table 4 of $\gamma_{\text{M}} = 15.3 \pm 0.7 \text{ km s}^{-1}$ and $K_{\text{M}} = 136.4 \pm 0.8 \text{ km s}^{-1}$. The uncertainties are the standard deviations of the four measurements with a small additional uncertainty in K_{M} to allow for the partial correlation of K_{M} with A . These values are both about 1.5 km s^{-1} lower than that obtained by fitting a simple sine wave to the data.

3.4 Spectroscopic orbit of the white dwarf

The measurement of the radial velocities for the white dwarf in RX J2130.6+4710 was difficult because there are only three spectral lines available to us which show a sufficiently sharp core to give reliable measurements. These spectral regions all show many sharp absorption lines and a strong, variable emission line from the M-dwarf. Fortunately, we have a spectrum of the M-dwarf alone obtained during an eclipse of the white dwarf. We are able to remove much of the contribution of the M-dwarf by subtracting this spectrum from the others. To do this, we first shift the wavelength scale of all the spectra to remove the orbital motion of the M-dwarf according to the orbit derived in section 3.3. The spectra were normalized by a constant value determined from the mean flux in the line wings. We interpolated the spectra onto three wavelength grids centered on each of the Balmer lines of 120 pixels of 32 km s^{-1} each. We then formed the average of spectra in groups taken at the same orbital phase to within 0.02 phase units.

We then subtracted from these 47 phase-binned spectra the spectrum obtained in eclipse scaled by some factor so as to optimize the removal of the sharp absorption features. This was done independently for each Balmer line as the optimum factor varies strongly with wavelength. For the $\text{H}\delta$ line we found that the spectrum obtained in eclipse was too noisy, so we used the combined spectrum of the M3 and M3.5 dwarfs LFT 1431 and LFT 1432 instead, which looked very similar but was much less noisy. The resulting spectra show the a strong absorption line near the line centre and the broad lines of the white dwarf with a weak core whose position varies sinusoidally with phase. In addition, some spectra show weak emission lines from the M-dwarf away from the line centre (Fig. 4) and the stronger central emission line from the M-dwarf which is not entirely removed by the subtraction process.

To measure the radial velocity of the white dwarf from these spectra, we created a model line profile for the white dwarf from the sum of three Gaussian profiles with the same mean but independent widths and depths. We then used least-squares fitting to the phase-binned spectra to determine the widths and depths of these Gaussians. Other parameters in the fit were the coefficients of a linear polynomial used to model the continuum and the width, height and position of a Gaussian used to model the emission line from the M-dwarf. Finding the optimum parameters for the Gaussians and the best scaling factor for the M-dwarf took much experimentation, but the quality of the fits achieved judged by the χ^2 value and by-eye is good. For the measured radial velocities reported here, we fixed the widths and depths of the Gaussians used to model the white dwarf spectrum to be the same for all the spectra. We then repeated least-squares fit to find the radial velocity of the white dwarf and the other free parameters of the fit. We also corrected for the shift applied to the spectra to correct them for the orbital motion of the M-dwarf. The phase-binned spectra around the $\text{H}\beta$ line, the model spectra and the residuals from the fit are shown in Fig. 4. Two phase-binned spectra of $\text{H}\beta$ observed near quadrature and the model spectra are also plotted in Fig. 5.

We used a least-squares fit to the measured radial velocities, V_r , of the function $V_r = \gamma_{\text{WD}} - K_{\text{WD}} \sin(2\pi[T - T_0]/P)$

Table 5. Results of least-squares fits of a sine wave to the measured radial velocities of the white dwarf in RX J2130.6+4710.

| Spectral line | γ_{WD} (km s^{-1}) | K_{WD} (km s^{-1}) | χ^2 ($n=47$) | σ (km s^{-1}) |
|---------------|--|---|------------------------|------------------------------------|
| H β | 39.2 ± 2.6 | 139.2 ± 3.4 | 43.0 | 17.9 |
| H γ | 58.4 ± 2.7 | 133.9 ± 3.8 | 43.1 | 21.4 |
| H δ | 51.7 ± 2.9 | 135.5 ± 4.1 | 52.7 | 22.3 |

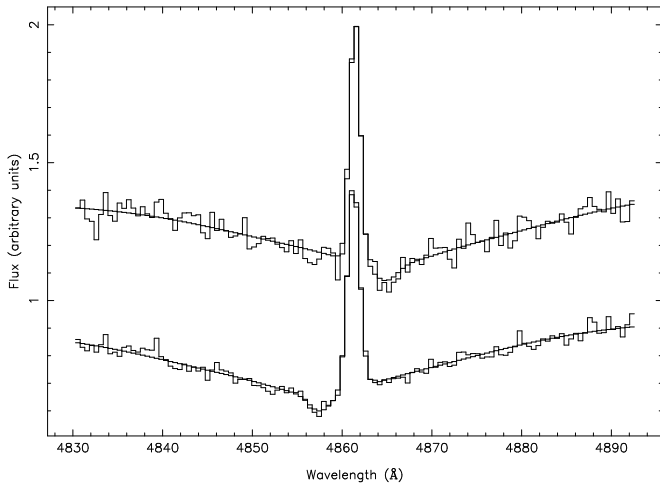


Figure 5. Examples of multiple Gaussian least-squares fits to the H β line. Two spectra of RX J2130.6+4710 which have had the M-star spectrum subtracted offset by 0.4 units are shown (thin line) together with the model spectra (thick line).

to measure the semi-amplitude of the spectroscopic orbit for the white dwarf, K_{WD} . The values of T_0 and the orbital period, P , were fixed using the ephemeris derived in section 3.1. Note that $\gamma_{\text{WD}} \neq \gamma_{\text{M}}$ for three reasons: *i.* the gravitational redshift of light from the white dwarf, $z = 0.635(M/M_{\odot})/(R/R_{\odot})\text{km s}^{-1} \approx 25\text{km s}^{-1}$; *ii.* the Stark effect is asymmetrical for the higher Balmer lines resulting in pressure shifts (Grabowski, Halenka & Madej 1987); *iii.* a tilt in the continuum will result in a systematic error in the value of γ_{WD} measured from such broad lines. The resulting fit for the H β line is shown in Fig. 6. Also shown are the radial velocities measured for the emission line, which are a by-product of the analysis. The values of γ_{WD} and K_{WD} measured from each Balmer line are given in Table 5. The agreement between the values of K_{WD} measured from the three lines is remarkably good, but we suspect this is a fluke. These values are certainly affected by systematic errors due to inaccurate subtraction of the M-dwarf spectrum, variable tilts in the spectrum and weak emission lines from the M-dwarf. Therefore, we should not take the error in the weighted mean as a measure of the uncertainty. Instead we use the standard deviation of the values and adopt the value $K_{\text{WD}} = 136.5 \pm 3.8 \text{ km s}^{-1}$.

3.5 The combined spectroscopic orbit

From the adopted value of P , K_{M} and K_{WD} we use Kepler's Law to derive the minimum masses, $m_{\text{M}} \sin^3 i$ and

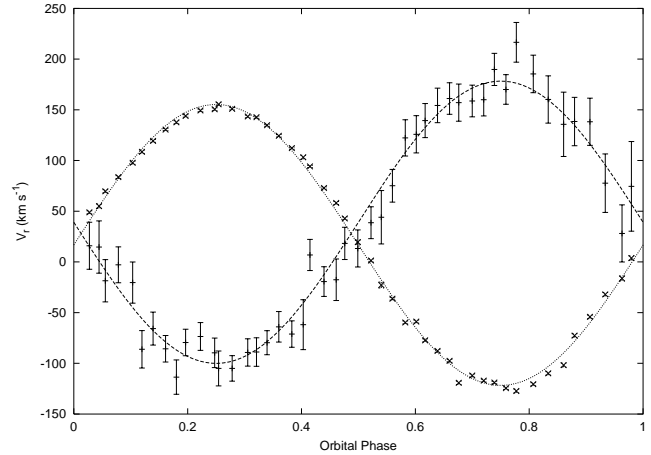


Figure 6. Radial velocities of the white dwarf (+) and the emission line from the M-dwarf (x) measured from the H β line. Sinusoidal least-square fits are shown as solid lines.

Table 6. The combined spectroscopic orbit of RX J2130.6+4710.

| Parameter | Value | Notes |
|----------------------------------|-----------------------------------|-----------------|
| T_0 | BJD 2 452 785.681876 | See section 3.1 |
| P | 0.521 035 625 d | See section 3.1 |
| γ_{WD} | 40 km s^{-1} | Uncertain |
| K_{WD} | $136.5 \pm 3.8 \text{ km s}^{-1}$ | |
| γ_{M} | $15.3 \pm 0.7 \text{ km s}^{-1}$ | |
| K_{M} | $136.4 \pm 0.8 \text{ km s}^{-1}$ | |
| $q = m_{\text{M}}/m_{\text{WD}}$ | 1.00 ± 0.03 | |
| $m_{\text{WD}} \sin^3 i$ | $0.548 \pm 0.016 M_{\odot}$ | |
| $m_{\text{M}} \sin^3 i$ | $0.549 \pm 0.022 M_{\odot}$ | |
| $a \sin i$ | $2.81 \pm 0.04 R_{\odot}$ | |

$m_{\text{WD}} \sin^3 i$, the mass ratio $q = m_{\text{M}}/m_{\text{WD}}$, and projected semi-major axis $a \sin i$, where m_{M} is the mass of the M-dwarf, m_{WD} is the mass of the white dwarf and i is the orbital inclination. The values derived and their uncertainties are given in Table 6. We have taken the value of γ_{WD} derived from the H β line as we believe this to be the least affected but systematic errors.

3.6 The lightcurve

The lightcurve of RX J2130.6+4710 shows that the white dwarf is eclipsed for 27 m 30 s and that the ingress and egress phases of the eclipse last for 1 m 50 s. The depth of the eclipse varies from 3.0 magnitudes in the u' band to less than 0.1 magnitudes in the I band (Fig. 8). There is no secondary eclipse apparent in our data, which is unsurprising given that it is expected to be less than 1 milli-magnitude deep. It is also noticeable that the amplitude of the reflection effect is rather small, i.e., the lightcurves are almost flat outside of the eclipse.

For a given inclination, i , a single eclipse will give an accurate measurement of the radii of the stars relative to their separation, i.e., $r_{\text{WD}} = R_{\text{WD}}/a$ and $r_{\text{M}} = R_{\text{M}}/a$, where a is the separation of the stars and R_{WD} , R_{M} are the radii of the white dwarf and the M-dwarf, respectively. Addition-

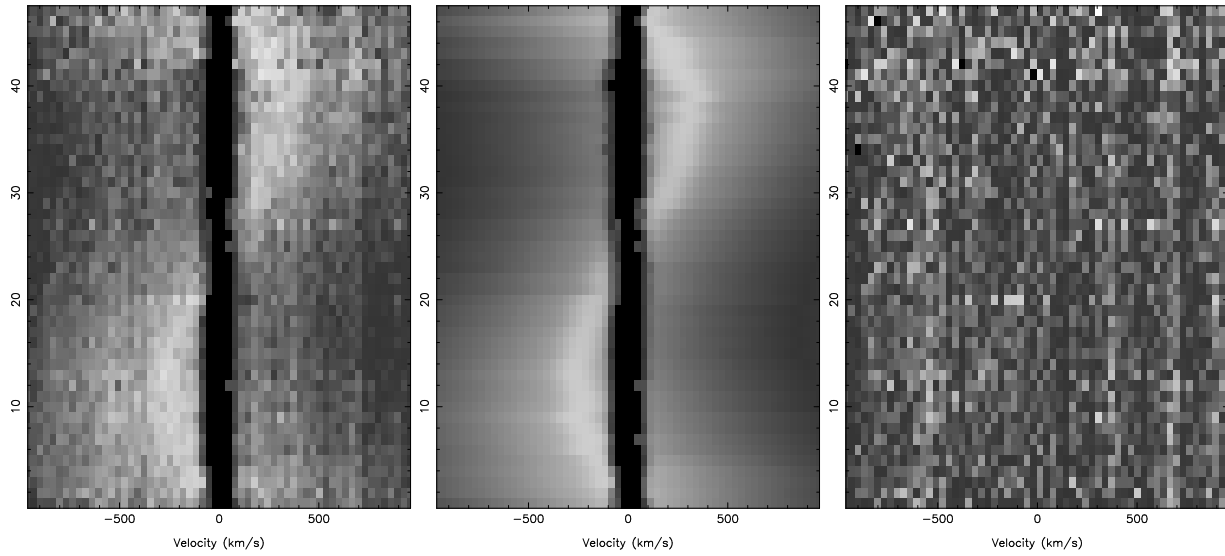


Figure 4. Trailed grey-scale spectra of the $H\beta$ line in RX J2130.6+4710. Left-to-right: observed, phase binned spectra after subtraction of the M-dwarf spectrum; least-squares fit; residuals from the fit. For the spectra, white is an intensity value of 0.5, black is 1.0. For the residuals the intensity scale is -0.1 to $+0.1$ from white to black.

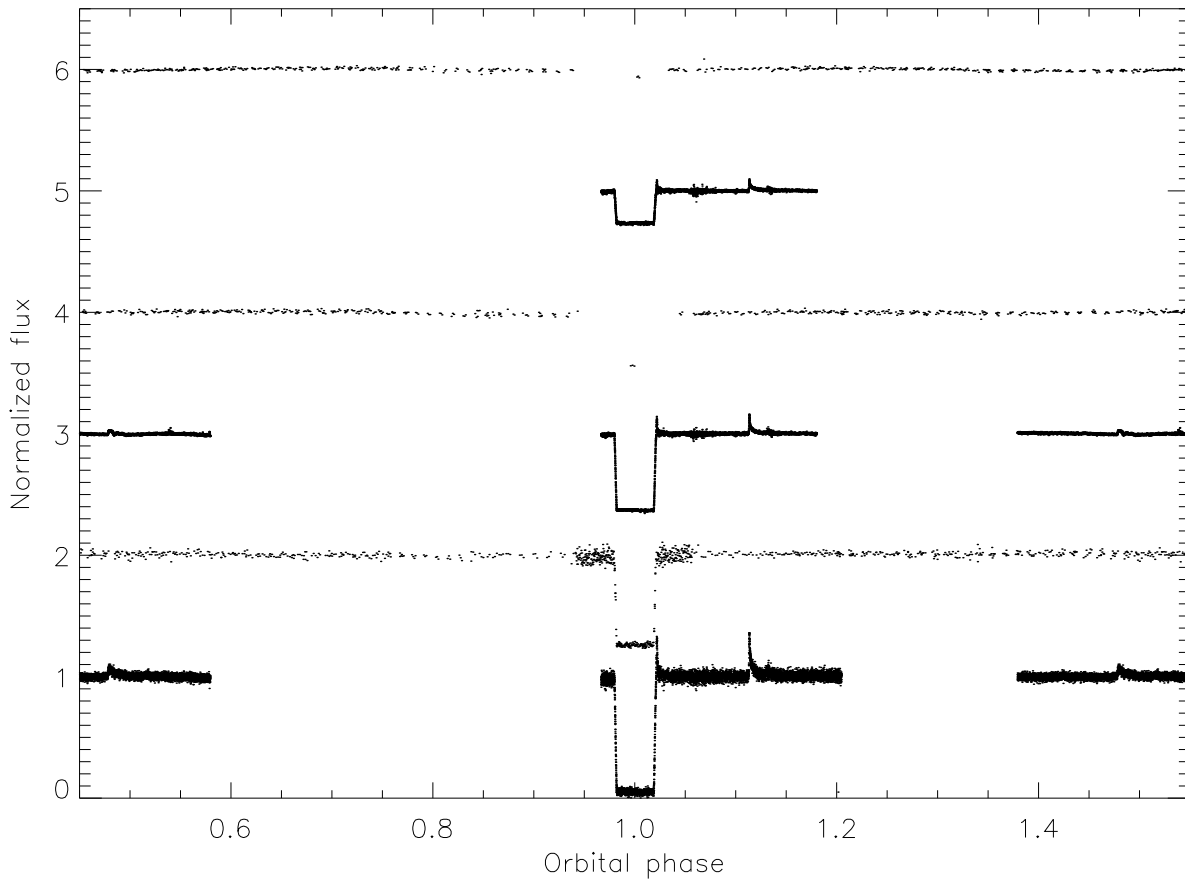


Figure 8. The lightcurves of RX J2130.6+4710 with the following filters (bottom to top); u' , B, g' , V, r' and I. The lightcurves have been normalized to the mean out-of-eclipse values and offset by 1.0 for clarity. The data for the u' , g' and r' filters around primary eclipse were obtained on the night 2002 May 17 and clearly show two flares. Data at other phases for the u' and g' bands were taken in poor seeing on the night 2003 November 13 and also shows two flares.

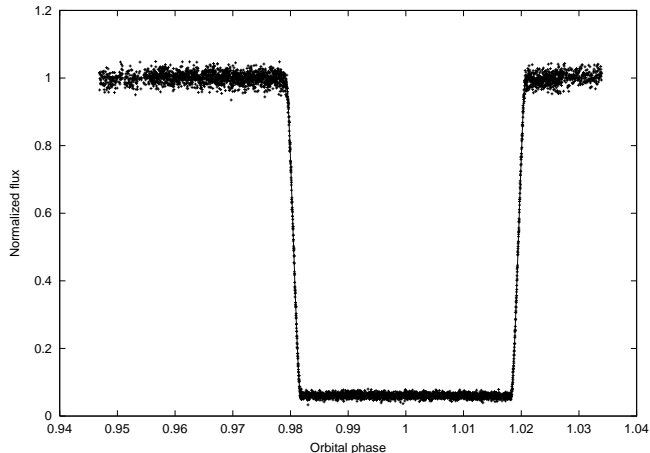


Figure 7. The lightcurve of RX J2130.6+4710 in the u' band (+) and the least-squares fit for the eclipse of uniform circular discs assuming $i = 80.5^\circ$ (solid line, barely visible).

ally, the depth of the eclipse gives an accurate measurement of the luminosity ratio, l_λ at the effective wavelength of the lightcurve λ . Equally good fits to the eclipse can be found for a wide range of i values. The shape of the M-dwarf is accurately determined by an equipotential surface in the Roche potential, which is slightly non-spherical. This gives rise to an ellipsoidal effect with an amplitude of about 2 percent in the I band lightcurve. The amplitude of the ellipsoidal effect varies strongly with r_M and the predicted value of r_M increases as i decreases, so we have enough information in the u' band and I band lightcurves to measure r_{WD} , r_M and i .

We first measured the values of r_{WD} and r_M as a function of i from the u' band lightcurve using the simple model of uniform circular discs described in section 3.1. We included data obtain on the night 2002 May 24 and 2002 May 25 in the fit after first normalising the data using a straight line fit to the data outside of eclipse. The results are plotted in Fig. 9. We used the slightly more advanced lightcurve model EBOP (Nelson & Davis 1972, Popper & Etzel 1981) to investigate the effect of limb-darkening on the values of r_{WD} and r_M derived, we find that this radii change by less than 0.1 percent if limb-darkening is included in the model.

We used a simple model to calculate the semi-amplitude of the ellipsoidal effect in the I band lightcurve, ΔI . The model creates a grid of points over an equipotential surface in the Roche potential. The observed flux as a function of phase is then calculated by numerical integration of the apparent surface brightness over the points visible at each phase. The apparent surface brightness over the star includes the effects of gravity darkening and limb-darkening. We calculated the value of ΔI as a function of i for linear limb-darkening coefficients of 0.63 and 0.72, which covers the range of values given in the tabulations of Claret (2000) for model stellar atmospheres with $T_{\text{eff}}=3500$ K. The gravity darkening exponent was fixed at its standard value of 0.08. The effect of gravity darkening is to make the lightcurve slightly fainter at phase 0 than phase 0.5. To calculate ΔI we used the semi-amplitude calculated from the flux at phase 0.5 because the data at phase 0 are affected by the eclipse of the white dwarf, although the difference is very small for

the amplitudes we are dealing with in this case. We also ignore the effect of the light from the white dwarf when we calculate ΔI , so a small correction for this contribution to the flux has to be made before comparing the predicted and observed values of ΔI . The predicted values of ΔI as a function of i are shown in Fig. 9.

The measurement ΔI is complicated by the asymmetry of the I band lightcurve, e.g., the minimum of the lightcurve does not occur at phase 0.5. We assume that this is due to the presence of spots on the surface of the M-dwarf. This is not an unreasonable assumption given that this is a rapidly rotating M-dwarf which is known to show flares (Fig. 8). To model this effect of these spots on the lightcurve, we assumed that there are two spots which cause dips in the lightcurve described by the functions $A_j(1 + \cos[\phi - \phi_j])/2$, $j = 1, 2$, which are restricted to orbital phases $\phi_j \pm \pi/2$. We modelled the ellipsoidal effect with the function $-\Delta I \cos(2\phi)$ and also included a component for the reflection effect using the function $-A_{\text{ref}} \cos(\phi)$. We first formed the average of the observations in phase bins 0.02 wide and calculated the standard deviation of the mean of the data in each bin. We then subtracted a constant to remove the contribution of the white dwarf to the measured flux and renormalised the data by its mean. The value of the constant is determined from the mean value of the observed flux during eclipse.

We then performed a weighted least-squares fit of the sum of the functions described above plus a constant to the phase-binned data excluding the data in eclipse to find optimum values of the parameters A_1 , A_2 , ϕ_1 , ϕ_2 , ΔI , A_{ref} and the constant. The resulting fit and the phase-binned data are shown in Fig. 10. With so many parameters, there will clearly be many solutions which give a good fit. In this case we are interested in finding the likely range of ΔI values which are reasonable given the observed lightcurve. To find the value of ΔI we attempted to fit the I band lightcurve with the dips due to the spots centered near phases 0.4 and 0.9 so as to remove as much of the variability as possible using the spots alone. The parameters for this fit are shown in Table 7.

The I-band data and the radial velocity data for the M-dwarf discussed in Section 3.3 were obtained simultaneously so the parameters for the dark spots we infer by modelling distortions to the lightcurve and radial velocity curve should be consistent. This is indeed the case for the phase of the distortion of the proposed spot with $\phi_1 \approx 0.4$ which is also responsible for the distortion to the radial velocity curve with $\phi_0 \approx 0.2$ since $\phi_1 \approx \phi_0 + \rho/2$. The radial velocity data near phase 0.8 are too sparse to confirm whether the value of $\phi_2 = 0.83$ for the second spot is reasonable. We can, in principle, check for consistency between the amplitudes of the distortions, but this is a less straightforward test (see Discussion below). We can at least point out that the size of the distortions to the I-band lightcurves are about 2 percent and that the distortion to the radial velocity curve is about 2 percent of the equatorial rotational velocity of the M-dwarf (51 km s^{-1}).

3.7 Masses and radii of the stars

From the lower panel of Fig. 9 we find that the observed value of $\Delta I = 0.0097 \pm 0.0024$ corresponds to an inclination of $i = (81.7 \pm 1.4)^\circ$. From the upper two panels we then

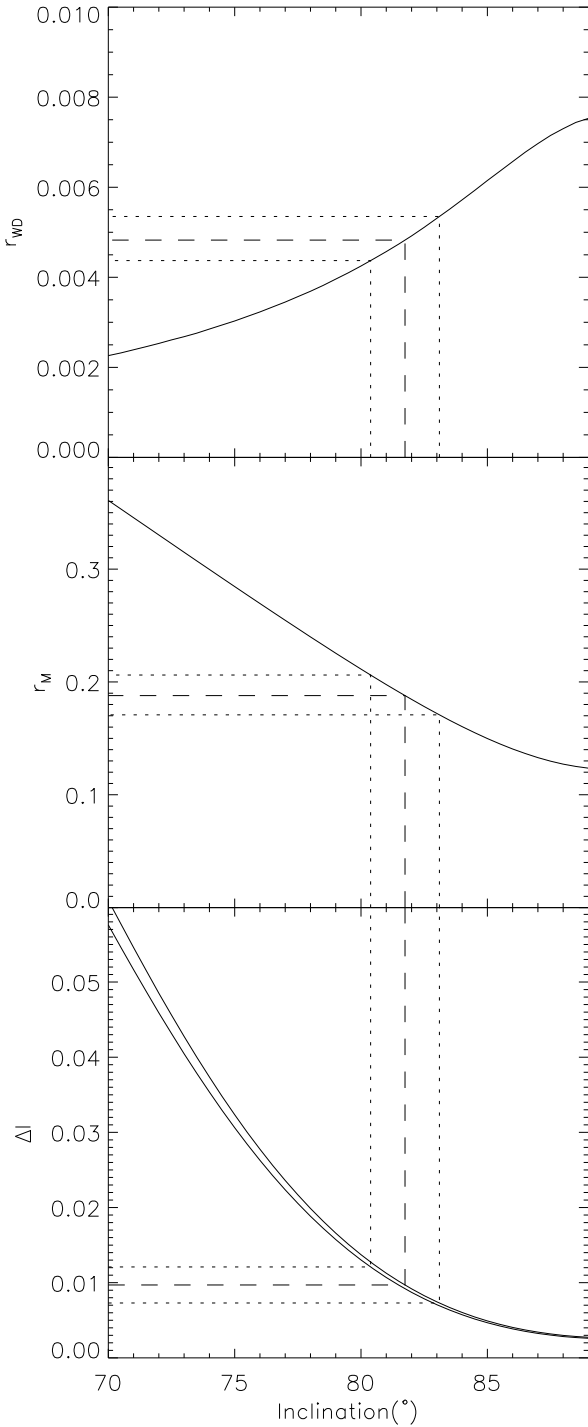


Figure 9. Upper panel: The optimum value of r_{WD} as a function of inclination from the least-squares fit to the u' band lightcurve; middle panel: optimum value of r_{M} ; lower panel: the predicted semi-amplitude of the I band lightcurve, ΔI for two values of the limb darkening coefficient. The conversion of the observed value of ΔI to values of r_{WD} and r_{M} and their uncertainties are illustrated by dashed and dotted lines, respectively.

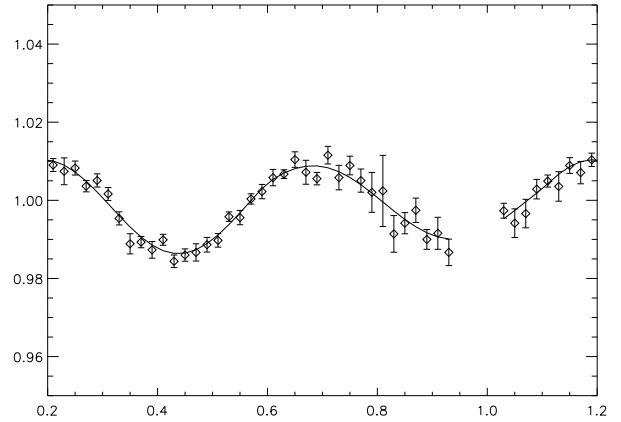


Figure 10. The phase-binned I band lightcurve of RX J2130.6+4710 with a model fit with two spot-like components, an ellipsoidal component and a reflection component.

Table 7. Parameters of the least-squares fit to the I band lightcurve.

| Parameter | Value |
|------------------|----------------------|
| Constant | 1.0103 ± 0.00053 |
| ΔI | 0.0097 ± 0.0024 |
| A_{ref} | 0.0010 ± 0.0009 |
| A_1 | 0.0175 ± 0.0012 |
| ϕ_1 | 0.369 ± 0.023 |
| A_2 | 0.0143 ± 0.0021 |
| ϕ_2 | 0.833 ± 0.022 |
| χ^2 | 40.86 |
| N | 46 |

find $r_{\text{WD}} = 0.0048 \pm 0.0005$ and $r_{\text{M}} = 0.188 \pm 0.018$. We combine these values with the combined spectroscopic orbit in Table 6 to derive the masses and radii for the stars given in Table 8. The positions of the stars in the mass-radius plane is compared to other white dwarfs and M-dwarfs in Fig. 11.

3.8 The effective temperature of the white dwarf

We compared the spectra of RX J2130.6+4710 to a grid of synthetic spectra calculated from pure hydrogen model atmospheres to estimate the effective temperature, T_{eff} , of the white dwarf.

Table 8. The masses, radii and effective temperatures of the stars in RX J2130.6+4710.

| Parameter | White dwarf | M-dwarf |
|------------------------|---------------------|-------------------|
| Mass (M_{\odot}) | 0.554 ± 0.017 | 0.555 ± 0.023 |
| Radius (R_{\odot}) | 0.0137 ± 0.0014 | 0.534 ± 0.053 |
| T_{eff} (K) | $18\,000 \pm 1000$ | 3200 ± 100^a |

^a Based on our estimate of the spectral type and the calibration of Leggett (1992).

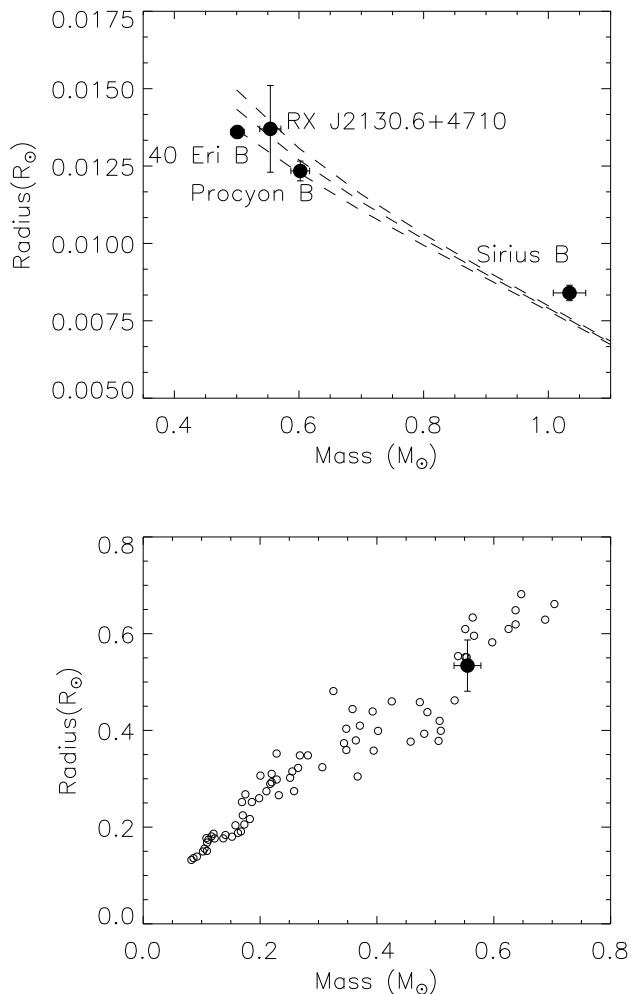


Figure 11. Upper panel: The white dwarf component of RX J2130.6+4710 in the mass-radius plane compared to other white dwarfs as labelled and the models of Benvenuto & Althaus (1999) for effective temperatures of 7500 K, 17000 K and 24790 K. Lower panel: The M-dwarf component of RX J2130.6+4710 in the mass-radius plane (filled circle) compared to other M-dwarfs (open circles) taken from Clemens et al. (1998).

These have been generated with the latest versions of the plane-parallel, hydrostatic, non-local thermodynamic equilibrium (non-LTE) atmosphere and spectral synthesis codes TLUSTY (version 200; Hubeny 1988, Hubeny & Lanz 2003) and SYNSPEC (version 48; Hubeny et al. 1985). All calculations include a full treatment of line blanketing and use a state-of-the-art model hydrogen atom incorporating the 8 lowest energy levels and one super-level extending from $n=9$ to $n=80$. During the calculation of the model structure, lines of the Lyman and Balmer series are treated by means of an approximate Stark profile. However, as we use the Balmer lines to determine the effective temperature and surface gravity of the white dwarf, it is important that we employ the best available line broadening data. Therefore, during the spectral synthesis step, detailed profiles for the H I lines are calculated from the Stark broadening tables of

Lemke (1997). We calculated synthetic spectra for model atmospheres over a range $15\,000\text{ K} < T_{\text{eff}} < 65\,000\text{ K}$ in steps of 5000 K and surface gravities in the range $6.5 < \log g < 8.5$ in steps of 0.5 ($\log g$ in cgs units.).

In order to compare the spectra of RX J2130.6+4710 to the model spectra, we first had to remove the contribution of the M-dwarf from the spectra. The spectra were normalized by a constant value determined from the mean flux around 4600 \AA . We interpolated the spectra onto a uniform wavelength grid of 2760 pixels over the wavelength range $3780\text{ \AA} - 5105\text{ \AA}$. We formed the average of spectra in groups taken at the same orbital phase to within 0.04 phase units. The phase ranges were chosen such that spectrum of RX J2130.6+4710 taken at mid-eclipse was in a group by itself. We calculated a scaling factor to apply to the mid-eclipse spectrum prior to subtracting it from each of the 24 phase-binned spectra by measuring the ratio of fluxes either side of the band head near 4954 \AA and the depth of the absorption feature near 4226 \AA . The scaling factor calculated was typically 0.25 at 4226 \AA and 0.36 at 4954 \AA . We multiplied the mid-eclipse spectrum by a linear function of wavelength fitted to these values prior to shifting it to account for the radial velocity then subtracting it from the phase-binned spectra.

We convolved the synthetic spectra with a Gaussian function to account for the resolution of the observed spectra and then interpolated the synthetic spectra onto the same wavelength grid at the phase-binned spectra. We were then able to compare the synthetic and observed spectra by calculating the χ^2 statistic for each combination of observed and synthetic spectrum. We did this separately for each Balmer line after applying a linear normalization calculated from the flux in the line wings to all the spectra. We excluded from the calculation of χ^2 a region $\pm 100\text{ km s}^{-1}$ wide centered on the Balmer emission lines from the M-dwarf, the Ca II H and K emission lines and an emission line near 3905.5 \AA which may be due to Si I.

For 20 of the phase-binned spectra the synthetic spectrum which gave the lowest value of χ^2 was calculated from model atmosphere with $T_{\text{eff}} = 20\,000\text{ K}$, $\log g = 8.0$. There is good agreement between the value of $\log g$ derived from fitting these spectra and the value calculated from the measured mass and radius, i.e., $\log g = 7.93^{+0.07}_{-0.09}$. Therefore, we created synthetic spectra corresponding to a range $15\,000\text{ K} < T_{\text{eff}} < 20\,000\text{ K}$ in steps of 1000 K and surface gravities of $\log g = 7.93, 7.84$ and 8.00 by interpolation over the synthetic spectra calculated from the model atmospheres. We calculated the χ^2 statistic for these interpolated spectra as before. We found that 17 of the spectra were best fit by model spectra with $T_{\text{eff}} = 18\,000\text{ K}$, $\log g = 7.84$ or $T_{\text{eff}} = 17\,000\text{ K}$, $\log g = 7.99$. These model spectra and a typical phase binned spectrum are shown in Fig. 12. The remaining 7 spectra were best fit by spectra within one grid-step of these two models. The quality of fits for spectra taken at phases from 0 to 0.5 judged by-eye and from the value of χ^2 is very good. The fits are not so good in the other half of the orbit if judged by the value of χ^2 (reduced χ^2 values ≈ 1.5). There is no reason for this which is obvious from an inspection of the fits, but it is probably due to a combination of inaccurate subtraction of the M-dwarf spectrum and inaccuracies in the flux calibration. The spectra in the phases range 0 to 0.5 tend to be fit best by spectra with $T_{\text{eff}} = 18\,000\text{ K}$. Therefore, we adopt an ef-

fective temperature of $T_{\text{eff}} = 18\,000\text{K}$ for the white dwarf in RX J2130.6+4710 and estimate that the uncertainty in this estimate is about 1000 K.

4 DISCUSSION

We can estimate the distance and reddening to RX J2130.6+4710 from its effective temperature and our B and V photometry. From the tabulations of Bergeron, Wesemael & Beauchamp we estimate that the white dwarf in RX J2130.6+4710 has an intrinsic color $(B-V)_0 = 0.00 \pm 0.02$ and an absolute V magnitude, $M_V = 11.0 \pm 0.1$. From the depths of the eclipses in the B and V bands combined with the photometry in Table 2 we can estimate apparent magnitudes for the white dwarf of $V=15.05 \pm 0.1$, $(B-V)=0.2 \pm 0.14$. From these values we estimate $E(B-V)=0.2 \pm 0.15$, $(m-M)=4.65 \pm 0.5$ and a distance to RX J2130.6+4710 of 85 ± 20 parsecs.

The distance to HD 204906 is known to be 82 ± 5 parsecs from its Hipparcos parallax (Perryman 1987). It would be fortunate if RX J2130.6+4710 could be shown to be physically related to HD 204906 because we could then measure accurate absolute magnitudes for the stars in this binary. Unfortunately, the measured radial velocity for HD 204906 is $34.8 \pm 1.4 \text{ km s}^{-1}$ (Sandage & Fouts 1987), which is very different from the value of $\gamma_M = 15.3 \pm 0.7$ we have measured. This suggests that HD 204906 and RX J2130.6+4710 are not physically related. One possibility that should be investigated is whether HD 204906 is itself a binary star.

The M-dwarf in RX J2130.6+4710 shows all the characteristics of a magnetically active star, i.e., soft X-ray emission, Balmer emission lines, flares and spots. We have attempted some crude modeling of the distortions to the radial velocity and lightcurves to account for these distortions. In reality, these spots are likely to be a complex pattern of dark regions with variations in the local temperature and the emergent spectrum. This pattern of dark regions can be approximated using models with circular spots, each with its own position (latitude and longitude), physical size and temperature. Modeling the two spots we have used to model the I-band lightcurve would therefore require eight free parameters plus some model for how the emergent spectrum depends on local temperature and viewing angle. This is not warranted given the quality of our data. Further observations of RX J2130.6+4710 with improved phase coverage and resolution could be used to study the pattern of active regions on the surface of the M-dwarf and the evolution of this pattern using techniques such as Doppler imaging (Rice 2002) or monitoring of the lightcurve. Such studies would benefit from the independent determinations of the rotational period of the star (assuming it is the same as the orbital period) the inclination of the star and the radius of the star presented here. This would, for example, allow a comparison of the rotational period derived from a Fourier analysis of the lightcurve excluding eclipses to the orbital period in order to look for asynchronous rotation in the M-dwarf. Monitoring of the eclipse times will then allow a further test of the mechanism proposed by Applegate (1992) to explain period changes in binaries similar to RX J2130.6+4710 such as V471 Tau. Indeed, the orbital periods of V471 Tau and RX J2130.6+4710 are very similar, so comparison of the re-

sults for these two stars will provide observational evidence for the way in which Applegate's mechanism depends on the mass of the magnetically active star.

In principle, a measurement of the depth of the secondary eclipse in RX J2130.6+4710 would allow a much more accurate determination of the masses and radii of the stars. Unfortunately, the predicted secondary eclipse depth is 7 milli-magnitudes or less. This will be very difficult to measure given the proximity of HD 204906 to RX J2130.6+4710 and the distortions to the lightcurve due to spots and flares. A more straightforward way to improve the accuracy of the masses and radii will be to obtain improved spectroscopy, both in terms of resolution and signal-to-noise, and to obtain a lightcurve at near infrared wavelengths where the measurement of the ellipsoidal effect will be less affected by star spots. High resolution spectroscopy at wavelengths of $3800 - 4000 \text{ \AA}$ may reveal sharp metal lines due to accretion of metals onto the surface of the white dwarf from the stellar wind of the M-dwarf (Zuckermann et al., 2002). These lines, if present, would allow the measurement of accurate radial velocities for the white dwarf and thus an accurate measurement of its gravitational redshift.

The spectral type of the M-dwarf in RX J2130.6+4710 is estimated to be M3.5Ve or M4Ve and its mass is $0.555 \pm 0.023 M_{\odot}$. This combination of mass and spectral type is not consistent with the calibration of Leggett (1992) for M-stars in the galactic disk. A typical M3.5V in the galactic disk has a mass of about $0.2 - 0.3 M_{\odot}$. An M-type star in the galactic disk with a mass of $0.55 M_{\odot}$ usually has a spectral type in the range M0V - M2V. This discrepancy may be due to an inaccurate estimate of the spectral type for the M-dwarf caused by using a limited spectral range with few features sensitive to spectral type and comparing this spectrum to stars which are not standard stars for the spectral class. A much more reliable estimate of the spectral type of the M-dwarf in RX J2130.6+4710 should be made using a spectrum taking during the eclipse covering the TiO bands in the regions $6000 \text{ \AA} - 9000 \text{ \AA}$. By contrast, the observed value of $(J - H) = 0.63$ is negligibly affected by the presence of the white dwarf and is typical for M-type stars in the galactic disk with a mass of $0.55 M_{\odot}$.

We have investigated the past and future evolution of RX J2130.6+4710 using the analysis described by Schreiber & Gänsicke (2003). The cooling age, t_{cool} of RX J2130.6+4710 derived by interpolating the cooling tracks of Wood (1995) is $\log(t_{\text{cool}}/y) = 7.85$. This is the time since RX J2130.6+4710 emerged from the common-envelope phase, at which time the orbital period is estimated to have been $0.53 - 0.6 \text{ d}$ depending on the prescription used to model the angular momentum loss due to a magnetic stellar wind in this interval. The continued loss of angular momentum will shrink the Roche lobe of the M-dwarf to the point where mass transfer will start from the M-dwarf to the white dwarf through the inner Lagrangian point. This will occur at an orbital period $P_{\text{sd}} = 0.185 \text{ d}$. Our estimate of the time before Roche lobe overflow occurs, t_{sd} , also depends on the prescription for angular momentum loss used and varies from $\log(t_{\text{sd}}/y) = 8.1$ to $\log(t_{\text{sd}}/y) = 9.6$. In either case, the time taken is less than a Hubble time so RX J2130.6+4710 can properly be described as a pre-cataclysmic variable star (pre-CV) in the sense defined by Schreiber & Gänsicke. The value of P_{sd} for RX J2130.6+4710 is well above the period

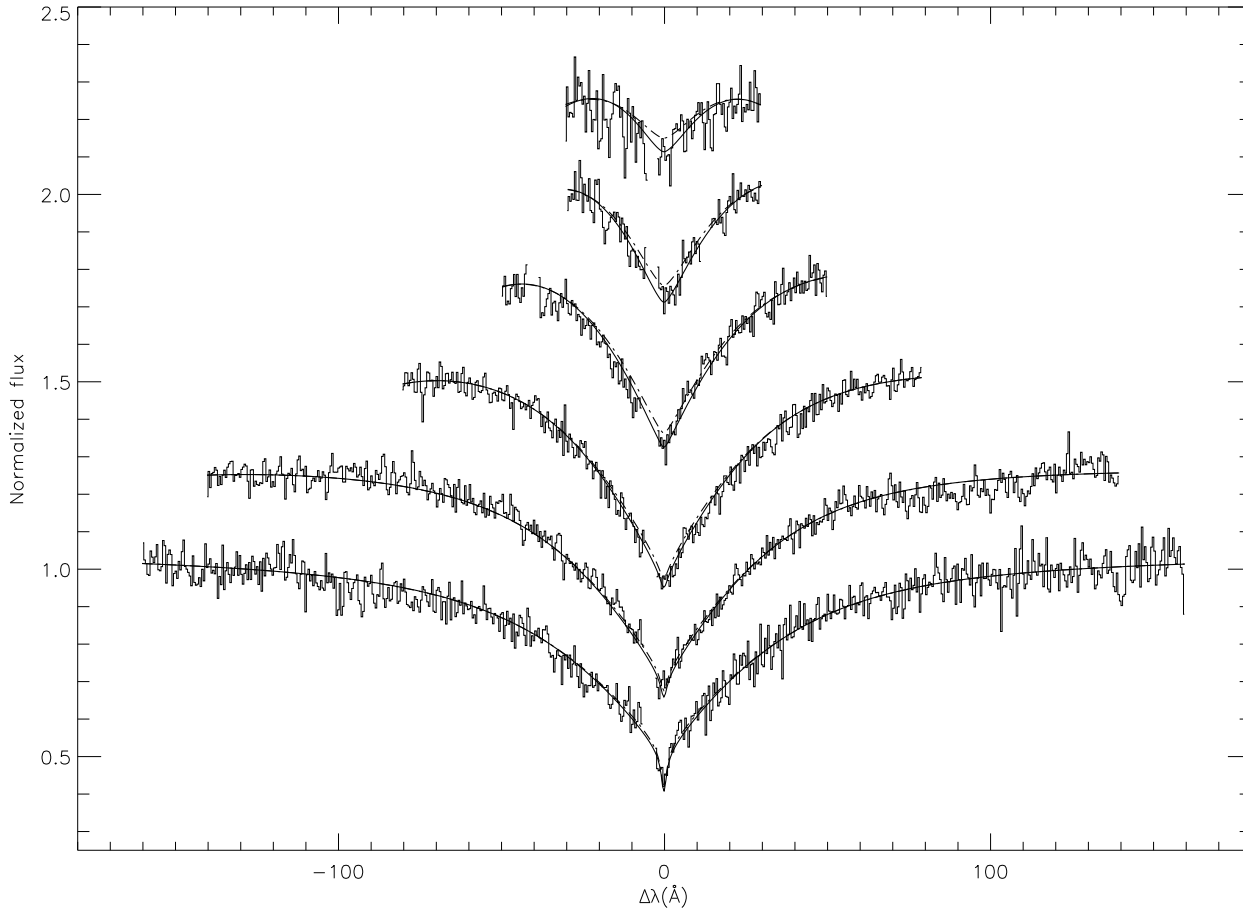


Figure 12. A typical phase-binned spectrum of the white dwarf in RX J2130.6+4710 plotted in sections offset by 0.25 around each Balmer line. The solid and dashed lines are synthetic spectra from model atmospheres with $T_{\text{eff}} = 18\,000\text{K}$, $\log g = 7.84$ and $T_{\text{eff}} = 17\,000\text{K}$, $\log g = 7.99$, respectively.

gap for CVs and is second only to V471 Tau among the systems compiled by Schreiber & Gänsicke. This implies that RX J2130.6+4710 is a member of the group of the rare progenitors of long orbital period CVs.

ACKNOWLEDGMENTS

PFLM and LMR were supported by a PPARC post-doctoral grant. The William Herschel Telescope, Isaac Newton Telescope and Jacobus Kapteyn Telescope are operated on the island of La Palma by the Isaac Newton Group in the Spanish Observatorio del Roque de los Muchachos of the Instituto de Astrofísica de Canarias. We would like to thank Romano Corradi for his prompt and informative reply to our query regarding the timing accuracy of data from the ING. This research has made use of the SIMBAD database, operated at CDS, Strasbourg, France. We thank an anonymous referee for their comments and suggestions regarding the modelling of distortions to the lightcurve and radial velocity curve.

REFERENCES

Applegate J.H., 1992, *ApJ*, 385, 621.

- Benvenuto, O.G., Althaus, L.G., 1999, *MNRAS*, 303, 30.
 Bergeron P., Wesemael F., Beauchamp A., 1995, *PASP*, 107, 1047.
 Claret, A., 2000, *A&A*, 363, 1081.
 Clemens J.C., Reid I.N., Gizis J.E., O'Brien M.S., 1998, *ApJ*, 496, 352.
 Dhillon V. S., Marsh T. R., 2001, *New Ast. Rev.*, 45, 91.
 Grabowski B., Halenka J., Madej J., 1987, *ApJ*, 313, 750.
 Harris D.E., Forman W., Gioia I.M., Hale J.A., Harnden Jr. F.R., Jones C., Karakashian T., Maccacaro T., McSweeney J.D., Primini F.A., Schwarz J., Tananbaum H.D., Thurman J., 1994, *EINSTEIN Observatory catalog of IPC X-ray sources, SAO HEAD CD-ROM Series I (Einstein)*, Nos 18-36.
 Hawley, S.L., Gizis, J.E., Reid, I.N., 1996, *AJ* 112, 2799.
 Hoard D.W., Wachter S., Clark L.L., Bowers T.P., 2002, *ApJ*, 565, 511.
 Hubeny I., 1988, *Computer Physics Comm.*, 52, 103.
 Hubeny I., Stefl S., Harmanec, P. 1985, *Bull. Astron. Inst. Czechosl.* 36, 214.
 Hubeny I., Lanz T., 2003, in *Stellar Atmosphere Modeling*, Eds. I. Hubeny et al., *ASP Conf. Ser.*, 288, 117.
 Iben I., Livio M., 1993, *PASP* 105, 1373.
 Jaschek C., Jaschek M., "The classification of stars", CUP, 1987.
 Landolt A.U., 1992, *AJ* 104, 340.
 Leggett S.K., 1992, *ApJS*, 82, 351.
 Lemke M., 1997, *A&AS*, 122, 285.
 Marsh, T.R., 1989, *PASP* 101, 1032.

- Motch C., Belloni T., Buckley D., Gottwald M., Hasinger G., Pakull M.W., Pietsch W., Reinsch K., Remillard R.A., Schmitt J.H.M.M., Trümper J., Zimmermann H.-U., 1991, *A&A*, 246, L24.
- Motch C., Guillout P., Haberl F., Pakull M. W., Peitsch W., Reinsch K., 1997, *A&A*, 318, 111.
- Naylor, T., 1998, *MNRAS*, 296, 339.
- Nelson, B., Davis, W.D., 1972, *ApJ*, 174, 617.
- Nidever, D.L., Marcy, G.W., Butler, R.P., Fischer, D.A., Vogt, S.S., 2002, *ApJS* 141, 503.
- Oke J.B., 1990, *AJ*, 99, 1621.
- Perryman, M.A.C., Lindegren, L., Kovalevsky, J., Hoeg, E., Bastian, U., Bernacca, P.L., Crz, M., Donati, F., Grenon, M., van Leeuwen, F., van der Marel, H., Mignard, F., Murray, C.A., Le Poole, R.S., Schrijver, H., Turon, C., Arenou, F., Froeschl, M., Petersen, C.S., 1997, *A&A*, 323, L49.
- Popper, D.M., Etzel, P.B., 1981, *AJ*, 86, 102.
- Press W.H. Teukolsky S.A., Vetterling W.T., Flannery B.P., 1992, *Numerical recipes in FORTRAN. The art of scientific computing*, 2nd edn. Cambridge University Press, Cambridge
- Reid, I.N., Hawley, S.L., Gizis, J.E., 1995, *AJ* 110, 1838.
- Rice J.B., 2002, *AN* 323, 220.
- Ritter H., Kolb U., 1998, *A&AS*, 129, 83.
- Sandage A., Fouts G., 1987, *AJ* 93, 592.
- Schneider, D.P., Young, P., 1980, *ApJ*, 238, 946.
- Schreiber, M.R., Gänsicke, B.T., 2003, *A&A*, 406, 305.
- Thompson R. J., Shelton R. G., Arning C. A., 1998, *AJ*, 115, 2587.
- Trümper J., 1983, *Adv. Space. Res.* 2, 241.
- Wallace, P.T., 2000, *SLALIB Programmer's Manual*, Starlink User Note, 67.61, CCLRC / Rutherford Appleton Laboratory (<http://star-www.rl.ac.uk/>).
- Wenger M., Ochsenbein F., Egret D., Dubois P., Bonnarel F., Borde S., Genova F., Jasniewicz G., Laloë S., Lesteven S., Monier R., 2000, *A&AS*, 143, 9.
- Wood, M.A., 1990, Ph.D. thesis, The University of Austin at Texas.
- Zuckerman B., Koester D., Reid I. N., Hünsch M., 2003, *ApJ*, 596, 477.